Sulfur-Incorporated ZIF67 as Efficient and Chloride-Resistant Bifunctional Catalysts for Alkaline Seawater Splitting

Sana Fathima T. K.[a], Sundara Ramaprabhu[a],*

[a]*Alternative Energy and Nanotechnology Laboratory,*

Department of Physics, Indian Institute of Technology

Madras, Chennai-36, Tamil Nadu, India

**Corresponding author: ramp@iitm.ac.in*

Abstract

In this work, we report sulfur-incorporated cobalt-based zeolitic imidazolate framework (ZIF67) composites as highly selective, chloride-resistant, efficient, and durable bifunctional catalysts for splitting alkaline seawater. The sulfur-incorporation has been carried out using two simple and scalable techniques: (a) melt-diffusion (ZIF67-S) and (b) in-situ addition (S@ZIF67), for comparison. The OER and HER activities of these catalysts are meticulously studied in 1 M KOH, simulated and alkaline seawater. The ZIF67-S sample exhibits the lowest OER overpotential (360 mV vs RHE at 10 mA cm^{-2}), HER overpotential (282 mV vs RHE at 50 mA cm^{-2}) and overall splitting voltage (1.86 V at 20 mA cm^{-2}) in alkaline seawater, owing to the synergistic effects of the metal active sites and the sulfur content. Post-electrolysis study is also carried out to probe the underlying mechanism involved in the catalysis.

Keywords: *Catalyst; ZIF67; OER; Electrolysis*

1. Introduction

Water electrolysis has recently gained attention for its ability to generate hydrogen, the most desirable clean energy carrier, without emitting CO_2 [1]. However, its development is limited by its high energy and water requirement. Splitting of natural water sources, such as ground water, seawater etc. has been recently explored as sustainable alternatives to curb the consumption of freshwater. Such natural water electrolysis is highly challenging due to the presence of impurities, which may lead to competing reactions and reduced efficiencies [1–3]. Among these sources, seawater is the most desirable due to its abundancy, yet is the most difficult to split due to its peculiar composition. The ions in it, specifically chloride ions, lead to sluggish and competitive reactions, and pose a threat of corrosion to the catalysts and catalyst supports [4]. Recent studies have focused on rationally designing catalysts that can tackle these challenges.

Since the major complexities associated with seawater electrolysis arise at the anode side, where the chlorine evolution reaction (ClER) competes with the sluggish oxygen evolution reaction (OER) [2,5], most of the reports focus on developing OER-selective, chlorine-resistant OER catalysts [2,4,6,7]. This typically requires OER catalysts with an overpotential value below 490 mV and an alkaline electrolyte, so as to avoid the influence of the chloride ions [8]. This is evident from the Pourbaix diagram for simulated seawater model reported by Dionigi et al. [9], which indicates that OER is thermodynamically favored over ClER at pH>7.5. Hence, an alkaline pH is chosen in this work. We had previously reported a cobalt-based zeolitic-imidazolate framework (ZIF67) derived Co-CoO@C nanocomposite as an effective OER catalyst in alkaline seawater with an overpotential (OER) of 374 mV at 10 mA cm^{-2} [5]. Its superior OER activities (low overpotentials, excellent selectivity, high stability, etc.) were attributed to the inherent characteristics imparted by the ZIF (a class of metal-organic framework) such as hierarchical porosity, abundant surface active sites, etc. and its optimal composition. In particular, its chloride corrosion resistance was due to its unique morphology which comprised of a protective nitrogen-rich amorphous carbon layer surrounding the catalytic nanoparticles. Although effective, this catalyst did not exhibit any activity towards the hydrogen evolution reaction (HER). HER also suffers from sluggishness in seawater due to the adsorption of multiple ions on the cathode [10]. Hence, it is necessary to rationally design suitable OER and HER, preferably bifunctional, catalysts to realize practical seawater electrolysis. Several catalysts such as transition metal based oxides, hydroxides, sulfides, etc. have been widely reported for overall seawater splitting [2,10–12].

A notable strategy to boost the efficiency and prevent corrosion is the doping of sulfur or sulfidation of transition metal-based nanocatalysts, wherein the presence of the electronegative S atoms or negatively charged sulfide anions (S^{2-}) can effectively repel the chloride ions (Cl^-) in seawater [13–15]. Such heterocatalytic structures comprise of multiple phase interfaces which can act as active sites and promote the catalysis [16]. The charge rearrangement at these interfaces also renders the adsorption strengths of the reaction intermediates on the active sites more favorable. The performance of the catalyst would depend on the sulfur incorporation process and parameters used, as a uniform, atomistic distribution of sulfur atoms or sulfide ions are desired on the electrode. For instance, Haq et al. [13] developed S doped Cu_2O-CuO nanoneedles as corrosion-resistant and efficient OER catalysts for seawater splitting. They reported a low overpotential of 420 mV at 500 mA cm^{-2} and excellent stability (~100 h) in alkaline seawater. The remarkable performance was attributed to the presence of S which boosted the kinetics, corrosion-resistance, and turnover frequency (TOF). Zhang et al. [17] reported nickel coated Cu_2S nanoarrays (on copper foam) for highly efficient HER in alkaline simulated seawater, with an overpotential of 200 mV at 500 mA cm^{-2} and stability of ~150 h. Here, the adsorption of the H intermediates on Ni was boosted by the strong Ni-S interactions. In another work [16], N and S co-doped carbon-coated Ni_3S_2/MoO_2 nanowires supported on nickel foam were reported as bifunctional catalysts for alkaline seawater splitting. They observed low overpotentials for OER (191 mV at 10 mA cm^{-2}) and HER (52 mV at 10 mA cm^{-2}), and overall splitting voltage (1.71 V at 100 mA cm^{-2}) in alkaline seawater. They noted that the heteroatom doping significantly enhanced the conductivity of the catalyst.

In this work, we report the development of novel sulfur incorporated ZIF67 composites as efficient bifunctional catalysts for alkaline seawater splitting. The incorporation of sulfur is carried out by two simple and scalable methods: (a) melt-diffusion method, and (b) in-situ addition. These techniques are much simpler, cost-effective, and utilize lower temperatures compared to the reported multi-step sulfidation or sulfur-doping methods. To the best of our knowledge, such scalable bifunctional catalysts based on sulfur-incorporated ZIF67 have not been reported yet for water or seawater splitting. The catalysts have been coated on cost-effective graphite felt substrates instead of metallic foam to avoid corrosion. The developed catalysts exhibit remarkable resistance to hypochlorite formation, high OER selectivity, good HER activity, and excellent stability in alkaline seawater.

2. Materials and Methods

The materials used for the synthesis and electrochemical studies are given in the Supplementary section S1.1.

2.1. Preparation of ZIF67

ZIF67 was prepared as reported previously [5]. Briefly, an 80 mL solution of 2-methylimidazole (in methanol, 45 mmol) was added to an 80 mL solution of cobalt nitrate hexahydrate (in methanol, 5.74 mmol). The resultant solution was stirred continuously at room temperature for 12 h. It was then filtered, subjected to methanol-washed twice, and dried at 60 °C to obtain a violet powder, termedas ZIF67.

2.2. Preparation of ZIF67-S

The sulfur incorporated ZIF67 (ZIF67-S) was prepared by a previously reported melt-diffusion technique with slight modifications [18]. Initially, ZIF67 and sulfur were taken in the ratio 2:1 and ground well for 1 h using an agate mortar and pestle. Further, the mixture was transferred to a quartz ampule and sealed. This was then loaded in a horizontal tubular furnace and heated to 155 °C at a rate of 5 °C/min. The sample was maintained at that temperature for 15 h, followed by natural cooling. The entire process was carried out under argon atmosphere. The resultant sample was labelled as ZIF67-S.

2.3. Preparation of S@ZIF67

In order to validate the efficiency of the melt-diffusion technique, sulfur incorporation was also carried out using a simple, in-situ modification of the ZIF67 preparation procedure. Briefly, 300 mg of sulfur was dissolved in 20 mL methanol and stirred well. This mixture was added to the cobalt nitrate solution before the addition of 2-methylimidazole solution. The rest of the procedure is similar to that of ZIF67. The resultant powder was labelled as S@ZIF67.

3. Characterization

3.1. Physical Characterization

The X-Ray Diffraction (XRD) pattern (Figure 1) of ZIF67-S indicates that it crystallizes in the characteristic cubic structure of ZIF67 (CCDC: 1429244), without any

impurities or additional peaks. From literature, it can be seen that such similar XRD patterns after modifications confirm the successful incorporation of the targeted moiety (such as dye, nanoparticles etc.) in the parent ZIF structure (here, S in ZIF67) [19,20]. On the other hand, the XRD pattern of S@ZIF67 (Figure 1) exhibits peaks corresponding to sulfur (AMCSD: 0010058) in addition to that of the ZIF structure. This indicates that the solution mixing method may not have been effective in incorporating the sulfur within the structure, and led to the formation of a sulfur-ZIF67 composite, with the sulfur molecules loosely attached to the structure.

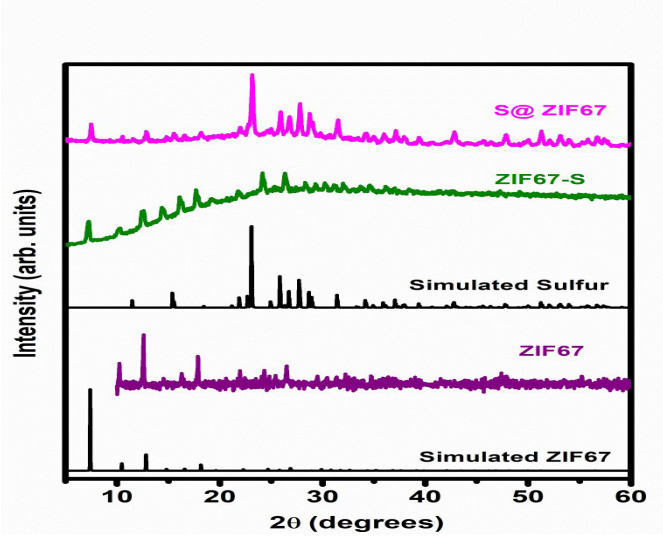


Fig. 1. XRD patterns of the synthesized catalysts

The sulfur incorporation was further validated from the thermogravimetric (TG) decomposition curves obtained in nitrogen atmosphere (Figure 2). The ZIF67 exhibits a two-step weight loss curve: first (~100 °C) corresponding to the loss of adsorbed moieties and a second (~450 °C) corresponding to the decomposition of the ligands in ZIF67 [5]. On the other hand, the ZIF67-S exhibits a weight loss region at ~155 °C corresponding to the sublimation of sulfur [18]. Based on this region, the sulfur loading content is estimated to be 40%. The S@ZIF67 exhibits additional weight loss regions, all of them corresponding to the loss of sulfur, but dependent on the strength of interaction between the sulfur and ZIF67.

The scanning electron microscopy (SEM) images of the samples are depicted in Figure 3. It can be observed that the ZIF67 exhibit micrometer-sized rhombic dodecahedrons, whereas the ZIF67-S has a heavily distorted yet smooth structure. The S@ZIF67 depicts structures similar to the parent ZIF67, with slight deformations and irregularities. The presence of sulfur in the prepared samples is also validated from their EDS spectra (Figure S1).

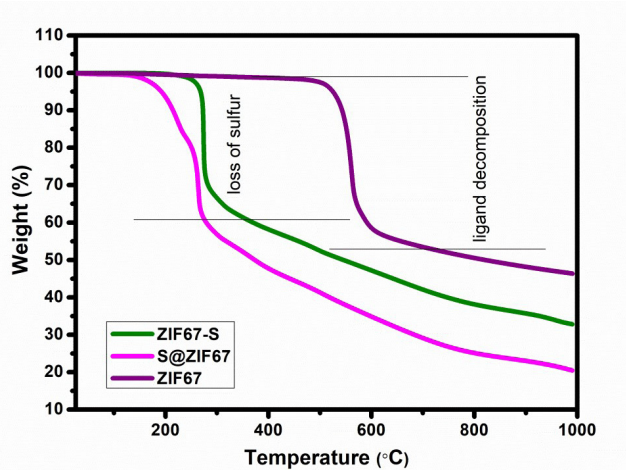


Fig. 2. TGA patterns of ZIF67, ZIF67-S, and S@ ZIF67

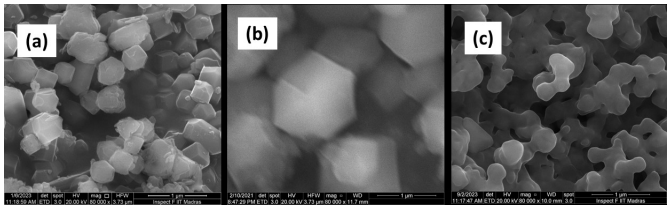


Fig. 3. SEM images of (a) ZIF67, (b) S@ZIF67, and (c) ZIF67-S

3.2. Electrochemical characterization

The OER activities of the prepared catalysts were initially assessed using the three-electrode mode. Before the measurement, the cyclic voltammograms (CV) of each catalyst/GF electrode was stabilized by running multiple cycles. The stabilized CV curves for ZIF67-S/GF are depicted in Figure S2a, and exhibit a pair of reversible redox peaks. This correspond to the M/M^{2+} and M^{2+}/M^{3+} redox couple, as discussed earlier [5]. This region is followed by a sharp increase in current density and simultaneous bubble formation, corresponding to oxygen evolution. Further, the iR-corrected linear sweep voltammograms (LSV) of all three catalyst/GFs obtained in 1 M KOH at a scan rate of 5 mV s^{-1} are depicted in Figure 4a. It is observed that the ZIF67-S/GF sample exhibited better OER activity compared to bare ZIF67 and S@ZIF67, with a remarkably low

overpotential (η) of 310 mV vs RHE at the benchmark current density of 10 mA cm^{-2}. This value is much lower than the cut-off of 490 mV to overcome the influence of chlorine in seawater, and hence is suitable for seawater electrolysis. Hence, the ZIF67-S/GF was further analyzed in simulated seawater (1 M KOH + 0.5 M NaCl) and alkaline seawater (seawater + 1 M KOH). The corresponding iR-corrected OER polarization curves are compared in Figure 4b. There is an obvious increase in the overpotential in seawater media (η_{10} = 360 mV vs RHE) due to the presence of multiple ionic moieties in it, specifically chloride ions. The η_{10} and η_{20} values in all three media are listed in Table 1.

Table 1: The OER η_{10} and η_{20} values of ZIF67-S/GF obtained in all three media

Catalyst/GF	η_{10} (mV vs RHE)	η_{20} (mV vs RHE)
1 M KOH	310	331
1 M KOH + 0.5 M NaCl	318	334
Seawater + 1 M KOH	360	386

To compare the kinetics of the catalyst/GFs, their Tafel slopes were calculated from the overpotential vs log j plots in 1 M KOH (Figure 4c). Both ZIF67/GF and S@ZIF67/GF exhibit a slope of ~89 mV dec^{-1}, indicating that the rate-determining step may be associated with the OH^- ion adsorption on the active sites. On the other hand, ZIF67-S/GF exhibits a lower slope of 51 mV dec^{-1}, indicating that the OH^- ion adsorption to M-O sites to form oxyhydroxide (M-OOH) may be the RDS in this case [21]. The lower Tafel slope of ZIF67-S/GF confirms its faster reaction kinetics compared to the other catalysts. In simulated and alkaline seawater (Figure 4d), ZIF67-S/GF exhibit Tafel slopes of 51.4 and 63.9 mV dec^{-1}, respectively. This may indicate a slightly slower kinetics in seawater medium, with the RDS being the adsorption of the OH^- ions to the M-OH sites [5].

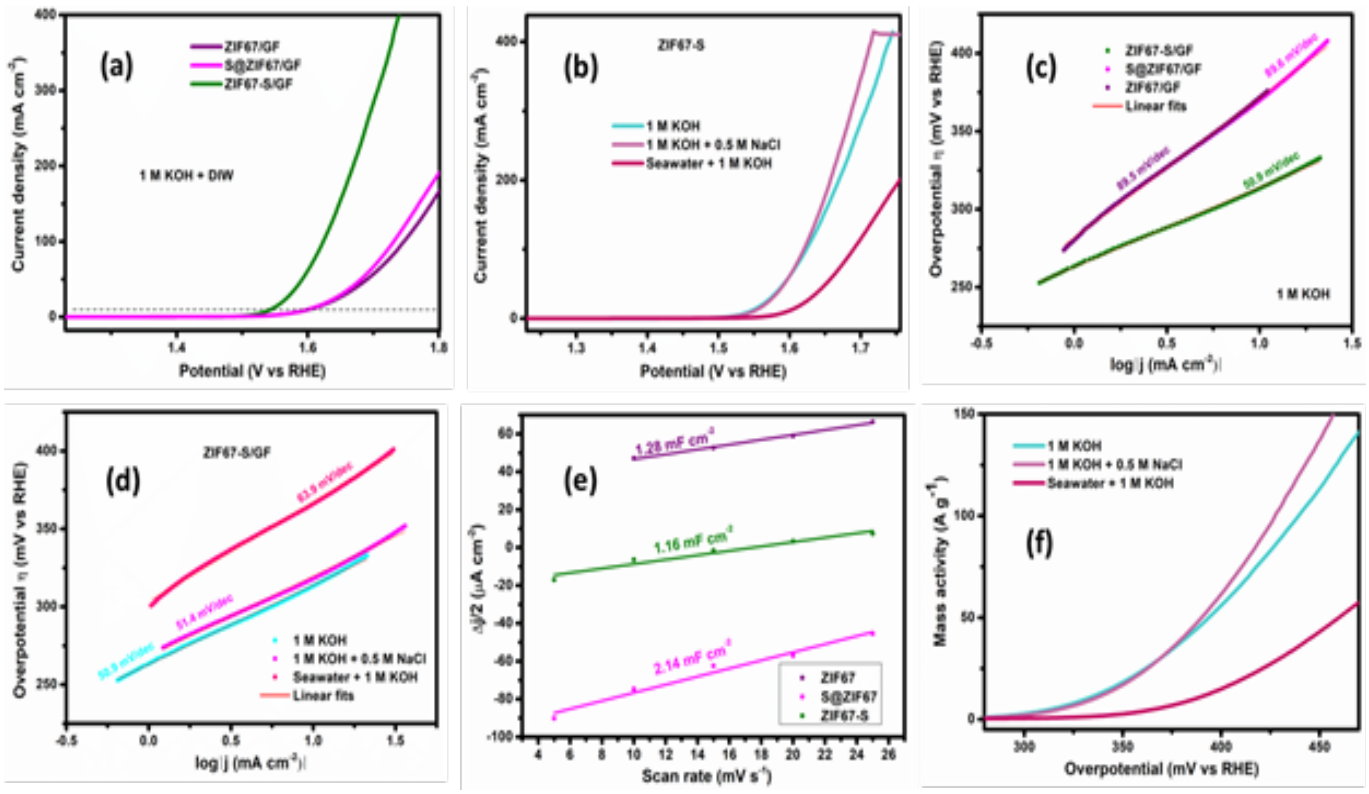


Fig. 4: (a) iR-corrected OER LSVs of the catalyst/GFs in 1 M KOH, (b) iR-corrected OER LSVs of ZIF67-S/GF in all three media, (c) Tafel slopes of the catalyst/GFs estimated in 1 M KOH, (d) Tafel slopes of ZIF67-S/GF in all three media, (e) C_{dl} values of the catalyst/GFs, and (f) mass activity of ZIF67-S/GF in all three media

Further, the electrochemical surface areas (ECSA) of the catalyst/GFs were estimated from the double layer capacitance values (C_{dl}) (Figures S3 and 4e) and are listed in Table 2. As reported earlier, the ECSA values do not seem to have an effect on the OER activity. The ZIF67-S/GF exhibits excellent mass activities (calculated as the current density divided by the catalyst loading (2 mg cm^{-2})) in all three media (Figure 4f).

To further correlate the performance of the catalyst/GFs, the concentration of the surface active sites was calculated (Supplementary section S1.4) from the area under the redox peaks observed in their CV in 1 M KOH (Figure S4) [5]. Higher surface active sites would imply more sites for the OER and HER reactions and faster kinetics. As seen in Table 2, the concentration varies as ZIF67-S/GF > S@ZIF67/GF > ZIF67/GF, validating the superiority of the melt-diffused ZIF67 sample (ZIF67-S).

Table 2: C_{dl}, ECSA, and surface concentration of active sites calculated for the catalyst/GFs

Catalyst/GF	C_{dl} (mF cm^{-2})	ECSA (cm^2)	Concentration of surface active sites (x 10^{16}) (cm^{-2})
ZIF67/GF	1.28	31.75	2.48
S@ZIF67/GF	2.14	52.92	4.39
ZIF67-S/GF	1.16	28.83	5.74

The activities of the catalyst/GFs towards HER were also measured in the three-electrode configuration. The stabilized CVs obtained prior to the polarization curves are shown in Figure S2b. In this case, the rapid increase in j along with bubble evolution corresponds to the hydrogen evolution at the electrode. The iR-corrected LSVs for HER of S@ZIF67/GF and ZIF67-S/GF in 1 M KOH (Figure 5a) depict a drastic improvement compared to ZIF67/GF. In our previous work [5], bare ZIF67/GF and ZIF67-derived materials did not show any activity towards HER. Interestingly, the incorporation of sulfur into the ZIF67 structure makes it active to HER, which may be attributed to the charge modulation occurring due to the strong interactions between the metal sites and sulfur [17]. The ZIF67-S/GF exhibits lower η_{50} value (321 mV vs RHE) compared to S@ZIF67 (402 mV vs RHE). The Tafel slope is also lower for ZIF67-S/GF (93 mV dec^{-1}) (Figure 5b). Hence, higher activity and faster kinetics for HER are observed for ZIF67-S/GF. The slopes obtained are in the range of 90 – 120 mV dec^{-1} which suggests that the RDS may be the Volmer step [10]. Further, the HER activities of the ZIF67-S/GF in simulated and alkaline seawater are shown in Figure 5c. The η_{50} and η_{100} values observed are listed in Table 3. It can be observed that the presence of ions boosts the HER activity, as it enhances the electrolyte conductivity. The Tafel slopes (Figure 5d) in this case also suggest that the Volmer step may be the RDS. The mass activities in all three media are expressed in Figure 5e.

Table 3: The HER η_{50} and η_{100} values of ZIF67-S/GF obtained in all three media

Catalyst/GF	η_{50} (mV vs RHE)	η_{100} (mV vs RHE)
1 M KOH	322	366
1 M KOH + 0.5 M NaCl	214	280
Seawater + 1 M KOH	282	350

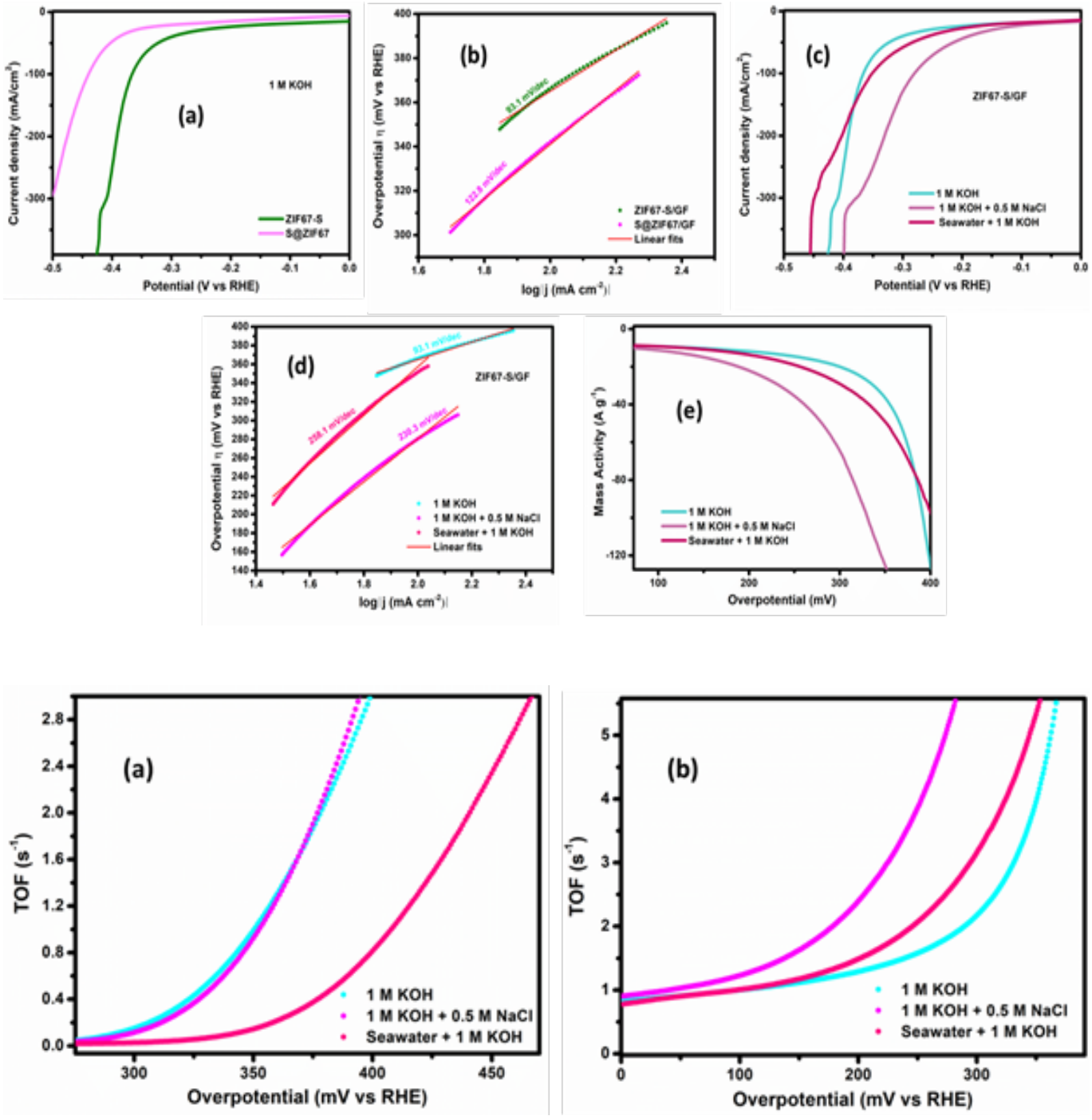


Fig. 5. (a) iR-corrected HER polarization curves and (b) Tafel plots of the catalyst/GFs in 1 M KOH, (c) iR-corrected HER polarization curves, (d) Tafel plots, and (e) mass activity of ZIF67-S/GF in all three media

The oxygen and hydrogen turnover frequencies (TOF) for ZIF67-S/GF calculated as described in Supplementary section S1.4 is depicted in Figure 6 (plotted versus overpotential). The TOFs obtained at specific overpotential values are listed in Table 4.

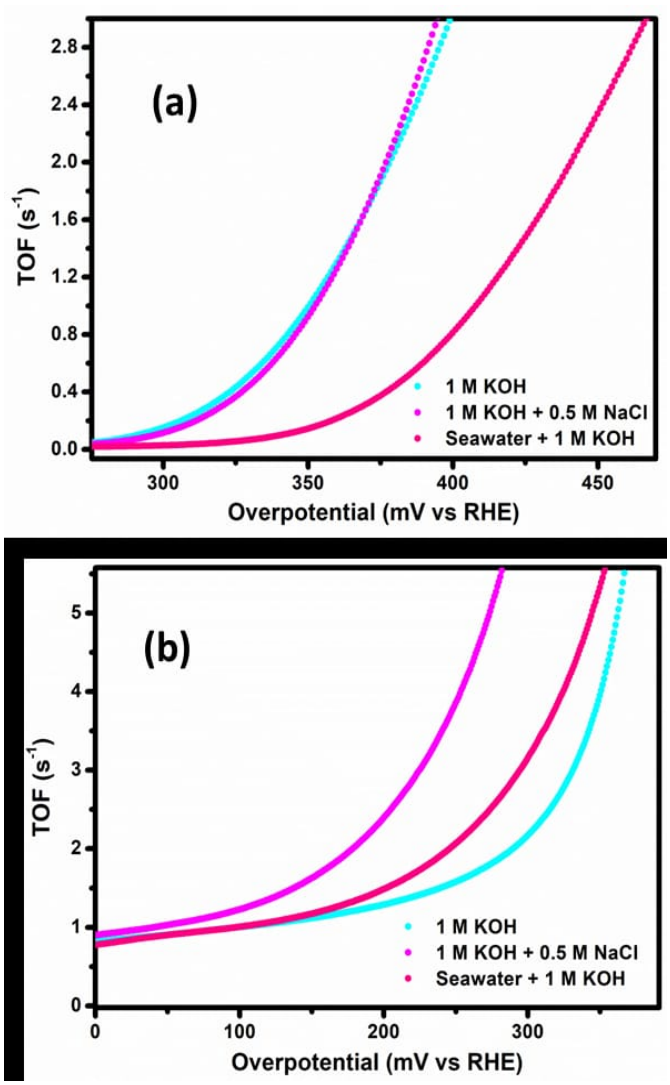


Fig. 6. (a) O_2 TOF and (b) H_2 TOF of ZIF67-S/GF in all three media

Table 4: The O_2 and H_2 TOF (s^{-1}) values of ZIF67-S/GF at specific overpotentials obtained in all three media

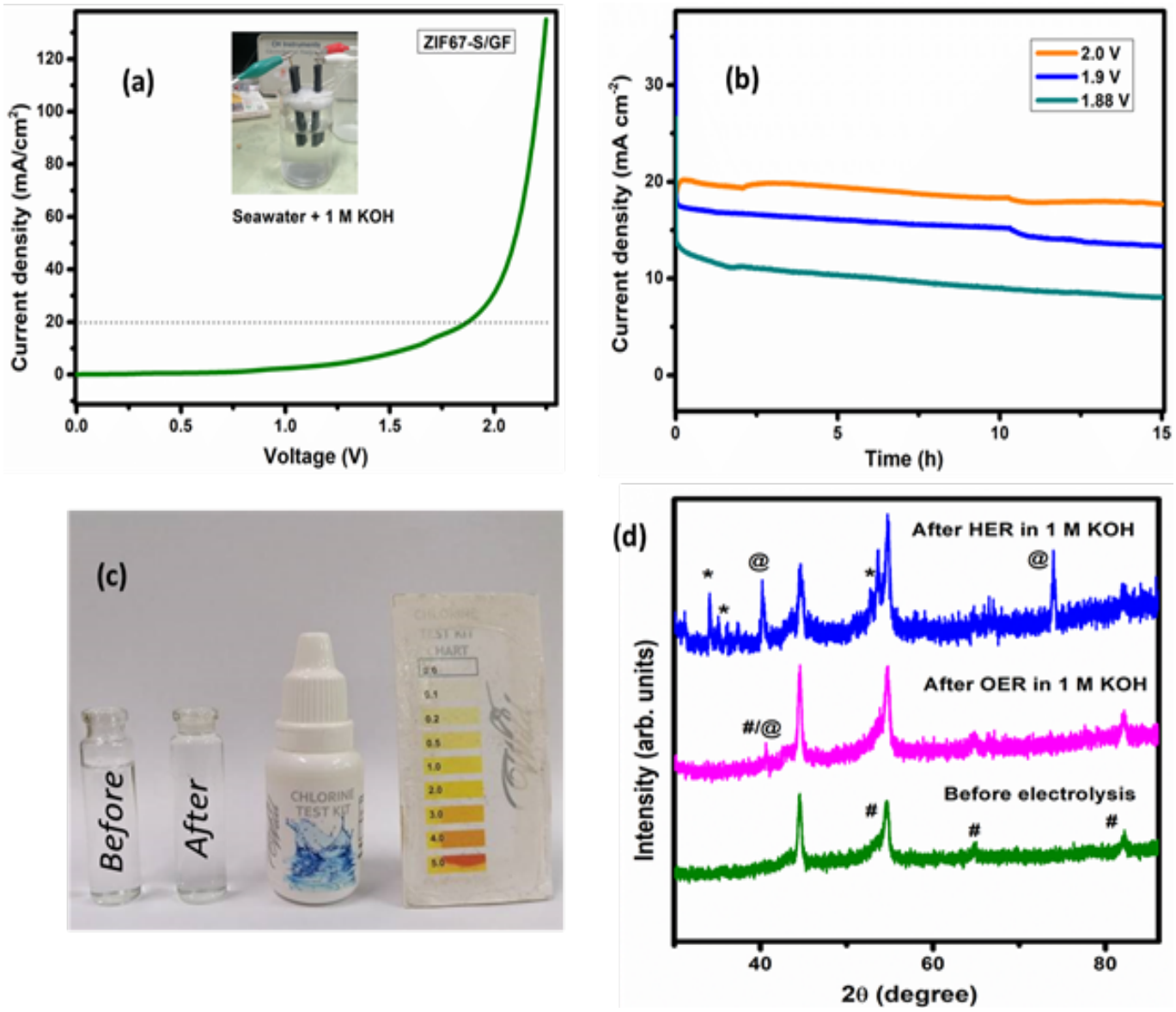
Catalyst/GF	O_2 TOF (s^{-1}) at η =		H_2 TOF (s^{-1}) at η=	
	310 mV	400 mV	200 mV	250 mV
1 M KOH	0.23	3.04	1.27	1.54
1 M KOH + 0.5 M NaCl	0.18	3.40	2.38	3.87
Seawater + 1 M KOH	0.03	0.82	1.46	2.10

3.3. Full-cell studies

Since the ZIF67-S catalyst exhibited superior performance for both OER and HER, it was considered further for the full-cell studies. The ZIF67-S/GF was taken as both anode and cathode, and the iR-corrected LSV was obtained in alkaline seawater (Figure 7a). A remarkably low overall splitting voltage of 1.86 V at 20 mA cm^{-2} (at room temperature) is observed for this ZIF67-S/GF||ZIF67-S/GF cell. For comparison, the iR-corrected LSV curve was also obtained in alkaline seawater using a standard combination of IrO_2/GF||Pt/C/GF (Figure S5). The overall splitting voltage obtained is 1.62 V at 20 mA cm^{-2}. This indicates that despite the absence of noble metals, the ZIF67-S catalyst can perform considerably well in alkaline seawater medium. The stability studies were also carried out in alkaline seawater at three different current densities (10, 15, and 20 mA cm^{-2}) for 15 h by the amperometric j-t technique. The ZIF67-S was coated on carbon paper (ZIF67-S/CP) for ease of post-electrolysis studies. Excellent stability is observed in all three cases (Figure 7b). To validate the efficacy of the catalyst for seawater electrolysis, the seawater after the stability study was subjected to a colorimetric hypochlorite detection test. As seen in Figure 7c, no colour change is observed after the addition of the reagent, which confirms the absence of hypochlorite.

3.4. Post-electrolysis studies

The ZIF67-S/CP after the stability study was subjected to post-electrolysis XRD to delve into the underlying origin of the splitting activity. As evident from Figure 7d, the original phase of the ZIF67-S is not observed in the patterns. The ZIF67 structure is known to immediately form a layer of cobalt oxide or oxyhydroxide on exposure to OH^- ions. Here, peaks corresponding to the fcc CoO structure (denoted by @) and Co_3O_4 (denoted by #) are observed, both before and after electrolysis [5]. This implies that a layer of CoO or Co_3O_4 may have formed during the coating process and further in-situ during the electrolysis. This in-situ formed layer further acts as the active layer for catalysis. The formation of this layer is also evident in the CV patterns of ZIF67-S/GF in all the media, i.e., the pair of redox peaks observed corresponds to the transformation of Co to CoO or Co_3O_4. Additionally, the pattern after HER comprises of a few unassigned peaks (denoted by *) which may be occurring due to the adsorption of several ions from the seawater [5].



Comparison of η_{OER}, η_{HER}, and overall splitting voltages of similar reported catalysts

Fig. 7. (a) Full-cell polarization curve obtained for ZIF67-S/GF||ZIF67-S/GF in alkaline seawater, (b) stability study of ZIF67-S/CP||ZIF67-S/CP at different applied voltages in alkaline seawater, (c) hypochlorite test before and after the stability study, and (d) post-electrolysis XRD of the coated electrode

4. Conclusion

In this work, sulfur-incorporated ZIF67 nanocomposites are reported as highly efficient bifunctional catalysts for alkaline seawater electrolysis. The ZIF67 sample with melt-diffused sulfur sample (ZIF67-S) exhibited superior performance for both OER and HER. Apart from the synergistic catalytic activity of the abundant Co or Co oxide active sites, this may also be attributed to the uniform distribution of the sulfur in the ZIF67 structure enabled by the melt-diffusion technique. The presence of the electronegative sulfur effectively repelled the chloride ions and boosted the OER selectivity and efficiency. In addition, sulfur incorporation also made the ZIF67 active towards HER, which may be due to the charge modulation arising from strong Co-S interactions. The ZIF67-S catalyst demonstrated comparable OER, HER, and overall seawater splitting performance than similar reported catalysts (Table 5). The HER activity

can be further improved by the incorporation of Ni or Mo sites. Optimizing the sulfur content can also considerably improve the performance, as a balance needs to be struck between repelling the undesirable chloride ions versus the adsorption intermediates. The developed catalyst is a highly efficient and economical substitute for current water splitting catalysts owing to its easy synthesis (two-step method with mild heat treatment; no noble metals) and low-cost precursors. We believe that this work can pave the way for the development of chloride-resistant, efficient bifunctional catalysts for alkaline seawater electrolysis.

Table 5: Comparison of η_{OER}, η_{HER}, and overall splitting voltages of similar reported catalysts

Catalyst	**Medium**	**η_{OER} (mV vs RHE)@ Current density (mA cm^{-2})**	**η_{HER} (mV vs RHE)@ Current density (mA cm^{-2})**	**Overall splitting voltage (V) @ j (mA cm^{-2})**	**Ref. (Year)**
S-(Ni,Fe)OOH/NF	Seawater + 1 M KOH	300@100	-	-	[22] (2020)
NiFe/NiS$_x$-Ni/NF	Simulated seawater	300@400	370@500	2.1@400	[23] (2019)
NiCoS/NF	Seawater + 1 M KOH	280@10	-	-	[24] (2021)
Ni_3N/Ni_3S_2/NF	Seawater + 1 M KOH + buffer	404@100	197@100	1.8@48.3	[25] (2019)
S-$NiMoO_4$@Ni-Fe LDH/NF	1 M KOH + Seawater	315@100	220@100	1.73@100	[26] (2022)
Co-CoO@C/GF	1 M KOH + Seawater	374@10	-	-	[5]
ZIF67-S/GF	*1 M KOH + Seawater*	*360@10*	*284@50*	*1.86@20*	*This work*

Acknowledgements

The authors acknowledge the Indian Institute of Technology Madras (IITM), India for financial support.

Reference

[1] Jiang S, Suo H, Zhang T, Liao C, Wang Y, Zhao Q, et al. Recent Advances in Seawater Electrolysis. Catalysts 12(2022) https://doi.org/10.3390/catal12020123.

[2] Mohammed-Ibrahim J, Moussab H. Recent advances on hydrogen production through seawater electrolysis. Mater Sci Energy Technol 3(2020):780–807. https://doi.org/10.1016/j.mset.2020.09.005.

[3] Kumar SS, Himabindu V. Hydrogen Production by PEM Water Electrolysis – A Review. Mater Sci Energy Technol 2 (2019) :442–54. https://doi.org/10.1016/j.mset.2019.03.002.

[4] Zhang F, Yu L, Wu L, Luo D, Ren Z. Rational design of oxygen evolution reaction catalysts for seawater electrolysis. Trends Chem 3(2021):485–98. https://doi.org/10.1016/j.trechm.2021.03.003.

[5] Fathima TKS, Ghosh A, Ramaprabhu S. ZIF67-derived Co–CoO@C nanocomposites as highly efficient and selective oxygen evolution reaction

(OER) catalysts for seawater electrolysis. Int J Hydrogen Energy 49(2023):780–93. https://doi.org/10.1016/j.ijhydene.2023.09.122.

[6] Yang J, Wang Y, Yang J, Pang Y, Zhu X, Lu Y, et al. Quench-Induced Surface Engineering Boosts Alkaline Freshwater and Seawater Oxygen Evolution Reaction of Porous NiCo2O4 Nanowires. Small 18(2022):1–9. https://doi.org/10.1002/smll.202106187.

[7] You H, Wu D, Si D, Cao M, Sun F, Zhang H, et al. Monolayer NiIr-layered double hydroxide as a long-lived efficient oxygen evolution catalyst for seawater splitting. J Am Chem Soc 144(2022):9254–63. https://doi.org/10.1021/jacs.2c00242.

[8] Jadhav AR, Kumar A, Lee J, Yang T, Na S, Lee J, et al. Stable complete seawater electrolysis by using interfacial chloride ion blocking layer on catalyst surface. J Mater Chem A 8(2020):24501–14. https://doi.org/10.1039/d0ta08543j.

[9] Dionigi F, Reier T, Pawolek Z, Gliech M, Strasser P. Design Criteria, Operating Conditions, and Nickel-Iron Hydroxide Catalyst Materials for Selective Seawater Electrolysis. Chem Sus Chem 9(2016):962–72. https://doi.org/10.1002/cssc.201501581.

[10] Mahmood N, Yao Y, Zhang JW, Pan L, Zhang X, Zou JJ. Electrocatalysts for hydrogen evolution in alkaline electrolytes: Mechanisms, challenges, and prospective solutions. Adv Sci 5(2018). https://doi.org/10.1002/advs.201700464.

[11] Ďurovič M, Hnát J, Bouzek K. Electrocatalysts for the hydrogen evolution reaction in alkaline and neutral media. A comparative review. J Power Sources 493(2021)4229708. https://doi.org/10.1016/j.jpowsour.2021.229708.

[12] Xie X, Du L, Yan L, Park S, Qiu Y, Sokolowski J, et al. Oxygen evolution reaction in alkaline environment: material challenges and solutions. Adv Funct Mater 32(2022)3. https://doi.org/10.1002/adfm.202110036.

[13] Haq T ul, Haik Y. S doped Cu2O-CuO nanoneedles array: Free standing oxygen evolution electrode with high efficiency and corrosion resistance for seawater splitting. Catal Today 400–401:(2022)14–25. https://doi.org/10.1016/j.cattod.2021.09.015.

[14] Haq T ul, Haik Y. Strategies of anode design for seawater electrolysis: Recent development and future perspective. Small Sci 2(2022); https://doi.org/10.1002/smsc.202200030.

[15] Jung SY, Kang S, Kim KM, Mhin S, Kim JC, Kim SJ, et al. Sulfur-incorporated nickel-iron layered double hydroxides for effective oxygen evolution reaction in seawater. Appl Surf Sci 568(2021)150965. https://doi.org/10.1016/j.apsusc.2021.150965.

[16] Fan X, Li B, Zhu C, Yan F, Zhang X, Chen Y. Nitrogen and sulfur co-doped carbon-coated Ni_3S_2/MoO_2 nanowires as bifunctional catalysts for alkaline seawater electrolysis. Small (2024)2309655:1–11. https://doi.org/10.1002/smll.202309655.

[17] Zhang B, Xu W, Liu S, Chen X, Ma T, Wang G, et al. Enhanced interface interaction in Cu_2S@Ni core-shell nanorod arrays as hydrogen evolution reaction electrode for alkaline seawater electrolysis. J Power Sources 506(2021)230235. https://doi.org/10.1016/j.jpowsour.2021.230235.

[18] Garapati MS, Ajay AP, Sundara R. Synergy between partially exfoliated carbon nanotubes-sulfur cathode and nitrogen rich dual function interlayer for high performance lithium sulfur battery. Carbon 147(2019)364–376. https://doi.org/10.1016/j.carbon.2019.03.007.

[19] Abdelhamid HN. Dye encapsulated hierarchical porous zeolitic imidazolate frameworks for carbon dioxide adsorption. J Environ Chem Eng 8(2020)104008. https://doi.org/10.1016/j.jece.2020.104008.

[20] Wang Z, Dou Z, Cui Y, Yang Y, Wang Z, Qian G. Sulfur encapsulated ZIF-8 as cathode material for lithium-sulfur battery with improved cyclability. Microporous Mesoporous Mater 185(2014)929–6. https://doi.org/10.1016/j.micromeso.2013.11.011.

[21] Anantharaj S, Ede SR, Karthick K, Sam Sankar S, Sangeetha K, Karthik PE, et al. Precision and correctness in the evaluation of electrocatalytic

water splitting: Revisiting activity parameters with a critical assessment. Energy Environ Sci 11(2018)1744–71. https://doi.org/10.1039/c7ee03457a.

[22] Yu L, Wu L, McElhenny B, Song S, Luo D, Zhang F, et al. Ultrafast room-temperature synthesis of porous S-doped Ni/Fe (oxy)hydroxide electrodes for oxygen evolution catalysis in seawater splitting. Energy Environ Sci13(2020)13439–45. https://doi.org/10.1039/d0ee00921k.

[23] Kuang Y, Kenney MJ, Meng Y, Hung WH, Liu Y, Huang JE, et al. Solar-driven, highly sustained splitting of seawater into hydrogen and oxygen fuels. Proc Natl Acad Sci U S A 116(2019)1624–1629. https://doi.org/10.1073/pnas.1900556116.

[24] Wang C, Zhu M, Cao Z, Zhu P, Cao Y, Xu X, et al. Heterogeneous bimetallic sulfides based seawater electrolysis towards stable industrial-level large current density. Appl Catal B Environ 291(2021)120071. https://doi.org/10.1016/j.apcatb.2021.120071.

[25] Zhao Y, Jin B, Vasileff A, Jiao Y, Qiao SZ. Interfacial nickel nitride/sulfide as a bifunctional electrode for highly efficient overall water/seawater electrolysis. J Mater Chem A 7(2019)8117–21. https://doi.org/10.1039/9ta01903k.

[26] Wang H, Chen L, Tan L, Liu X, Wen Y, Hou W, et al. Electrodeposition of NiFe-layered double hydroxide layer on sulfur-modified nickel molybdate nanorods for highly efficient seawater splitting. J Colloid Interface Sci 613(2022)349–58. https://doi.org/10.1016/j.jcis.2022.01.044.